Specular and diffuse reflectivity from thin films containing misfit dislocations

P.F. Miceli[a,*], J. Weatherwax[a], T. Krentsel[a], C.J. Palmstrøm[b]

[a] Department of Physics and Astronomy, University of Missouri-Columbia, Columbia, MO 65211, USA
[b] Department of Chemical Engineering and Materials Science, University of Minnesota, Minneapolis, MN 55455, USA

Abstract

We discuss the effects of misfit dislocations on the specular and diffuse scattering observed in X-ray reflectivity at the Bragg reflections of thin films. Using experimental results from ErAs/GaAs(0 0 1), it is shown that an interfacial displacement-difference correlation function can be used to model the scattering from misfit dislocations. We find that the diffuse scattering is correlation-length-limited for weak disorder whereas it has a rotational character for strong disorder. It is suggested that the correlation length arises from the elastic image field of a misfit dislocation.

X-ray and neutron reflectivity measurements, performed at grazing angles as well as near Bragg reflections, often seek information on the positional fluctuations of buried interfaces. Although displacement of these interfaces will arise from interdiffusion or natural fluctuations (i.e., kinetic roughening) which occur during film growth, extended crystalline defects also contribute displacements. Even in this films grown by molecular beam epitaxy (MBE) where interface roughening is relatively small, one expects displacement fluctuation contributions from misfit dislocations for films deposited on dissimilar substrates. Therefore, misfit dislocations should be observable in reflectivity measurements, although, the extent to which they can be observed may depend on the relative importance of other contributions and on the conditions of the reflectivity measurement.

Dislocations in large extended crystals often lead to disorder that is rotational in character and it causes a broadening of the diffraction line shapes into arcs in reciprocal space [1]. This occurs for a variety of dislocation distributions – for example, arrays of dislocations that form small angle tilt boundaries as well as random distributions of dislocations [2]. Such 'mosaic crystals' are commonly observed and the scattering can be

described by adding the intensity from each of many small mosaic blocks constituting the crystal.

It has recently been demonstrated that, unlike conventional mosaic crystals, thin films can possess *weak* disorder which leads to a two-component line shape (specular and diffuse scattering) measured transverse to a specular Bragg position [3]. There are now a number of experimental studies which observe these line shapes from metal [4–8] as well as semiconductor [9] epitaxial films containing misfit dislocations. In this paper, we focus on how the strength of disorder in a thin film affects the diffuse scattering and we show that: (1) weak disorder leads to diffuse scattering which is characteristic of the defect length scale; (2) strong disorder leads to diffuse scattering arising from the short range correlations of the defect displacement fields, similar to a conventional mosaic crystal; and (3) an elastic image field of the defect, due to a stress-free surface, determines the lateral defect size.

Fig. 1 illustrates the essential phenomenology of the line shapes for thin films of ErAs(0 0 1) grown [10] on GaAs(0 0 1) where both the lattice relaxation [9] and growth morphology [11, 12] have been studied extensively by X-ray scattering. For the present investigation, this system has the advantage that the misfit dislocation separation is conveniently controlled by the film thickness [9]. The X-ray measurements were performed using MoK$_{a_1}$ radiation from a rotating anode source along

* Corresponding author.
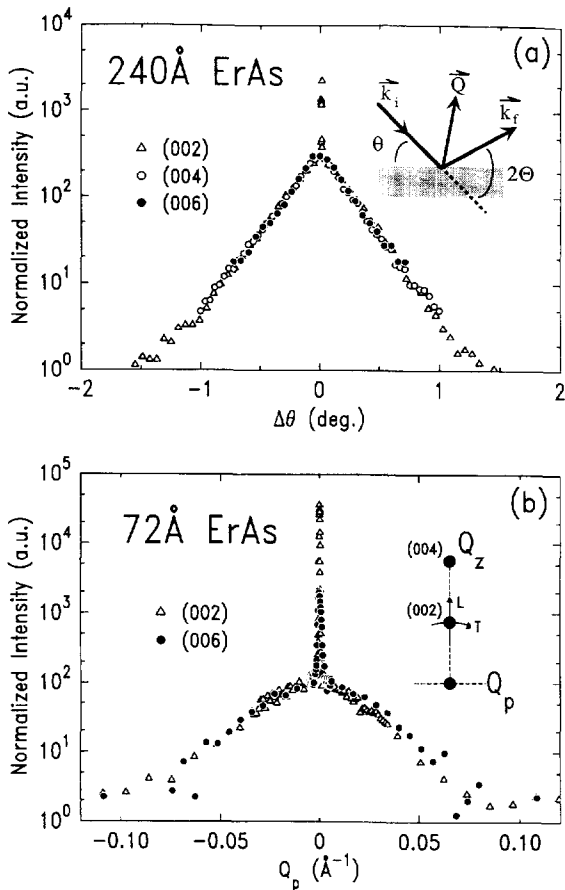
Fig. 1. (a) Transverse scans through specular Bragg reflections are shown for a 240 Å film of ErAs ($\Delta\theta \equiv \theta - \Theta$). Only the (0 0 2) exhibits a resolution limited component and the angular width of the diffuse scattering is same at each Bragg position. (b) Similar scans for a 72 Å film of ErAs. The data are plotted versus parallel scattering vector and the diffuse scattering has the same width at each Bragg position. The resolution limited component is much stronger than in (a). The inset to (a) shows the scattering geometry and the inset to (b) shows the scan directions in reciprocal space. 'T' is a transverse scan (essentially parallel to the surface) and 'L' is a longitudinal scan (perpendicular to the surface).

with Ge(1 1 1) monochromater and analyzer crystals arranged nondispersively. Shown are transverse scans through the Bragg positions located along the surface normal – the measurement geometry and scan direction in reciprocal space are given in the insets of Fig. 1.

In Fig. 1(a), a 240-Å-thick film of ErAs exhibits a two component line shape at the (0 0 2) position: there is a narrow, resolution limited (< 0.003°) feature occurring at the specular condition ($Q_p = 0$) as well as diffuse scattering which has a peak intensity an order of magnitude

weaker. The narrow component is not observed at higher order Bragg positions. To illustrate the scaling of the diffuse line shapes, the intensities have been normalized by a constant factor. It is seen that the *angular* width of the diffuse scattering is independent of the perpendicular scattering vector, Q_z, and this suggests that the disorder is rotational in nature. However, these data cannot be explained in terms of a conventional mosaic crystal as it does not allow for the narrow feature at the (0 0 2).

Fig. 1(b) shows the results for a 72-Å-thick film of ErAs. In this case, a narrow component is observed at both the (0 0 2) and (0 0 6) positions. Furthermore, the diffuse line shapes behave quite differently than in Fig. 1(a): measured in units of the parallel scattering vector, Q_p, the diffuse width is independent of Q_z. The width of the diffuse scattering suggests that the disorder has a characteristic correlation length on the order of ∼ 130 Å.

We now discuss the origin of the diffuse scattering widths as well as the two component line shape observed in Fig. 1. Before proceeding, it is worth noting that the dislocation density, thus the degree of disorder, is much larger for the 240 Å film than for the 72 Å film. It is known [9] that the dislocation separation and the specular intensity both decrease with increasing film thickness.

To construct a scattering model we need to know the displacement fields, u, arising from the defects. This is simplified by the experimental observation [3] that the displacements producing the diffuse scattering are vertically uniform and originate from the film–substrate interface. The result is quite reasonable given that we expect misfit dislocations to be located at this interface in order to accommodate the lattice mismatch, and that the stress-free surface of a thin film can lead to vertically homogeneous strain. We utilize these displacements and, in order to focus on issues related to the defect scattering, we neglect the scattering from the substrate and the film surface roughness so that the differential scattering cross-section for the thin film [12] is given as

$$\frac{d\sigma}{d\Omega} = n_A b^2 A_{ir} \frac{\sin^2(N_z Q_z c/2)}{\sin^2(Q_z c/2)} \sum_r e^{iQ_p \cdot r} \langle e^{iQ \cdot [u(r) - u(0)]} \rangle, \quad (1a)$$

where N_z is the number of lattice planes with spacing, c, A_{ir} is the irradiated area, n_A is the number of atoms per area, and b is the scattering length. Q is the scattering vector with components Q_z and Q_p along the film normal and in the film plane, respectively. r is a relative coordinate for the atomic positions in the film plane and the average, $\langle \ \rangle$, is taken over all possible origins. Although not essential, it is convenient to approximate the displacements as a Gaussian random variable [13]. This has the advantage of clarifying our discussion of the displacements by reducing them into a single displacement-difference correlation function, $2\sigma^2(r) = \langle [u_z(r) - u_z(0)]^2 \rangle$,

along the film normal (the effect of the approximation is discussed below). Now we obtain

$$\frac{d\sigma}{d\Omega} = (2\pi n_A b)^2 A_{ir} \frac{\sin^2(N_z Q_z c/2)}{\sin^2(Q_z c/2)} [\Gamma_{spec}(Q) + \Gamma_{diff}(Q)],$$

(1b)

$$\Gamma_{spec}(Q) = e^{-Q_z^2 \sigma^2(\infty)} \delta(q_p),$$

$$\Gamma_{diff}(Q) = \frac{1}{(2\pi)^2} \int d^2 r e^{iq_p \cdot r} [e^{-Q_z^2 \sigma^2(r)} - e^{-Q_z^2 \sigma^2(\infty)}],$$

where $q_p = Q_p - G_p$ and G_p is the in-plane component of any reciprocal lattice vector. It is assumed that Q_p is in the vicinity of a particular G_p. For the specular Bragg positions considered here, $G_p = 0$.

There are two Q-dependent multiplicative factors in Eq. (1), with the first giving thin film interference fringes along the longitudinal direction. At the Bragg position, this factor is just N_z^2. The second factor is the transverse line-shape which exhibits both narrow and diffuse components. The narrow component, $\Gamma_{spec}(Q)$, is attenuated by a Debye–Waller-like factor resulting from the root-mean-square (rms) displacements, $\sigma(\infty)$. This explains why the intensity of the narrow component decreases with increasing scattering vector in Fig. 1 and it also explains why the narrow components are stronger for the thinner film which has weaker disorder (smaller $\sigma(\infty)$).

The nature of the diffuse line shape, $\Gamma_{diff}(Q)$, also depends on $\sigma(\infty)$, so we first consider the behavior of $\sigma(r)$ shown schematically in Fig. 2. As $r \to 0$, the height fluctuations arise from displacements *within* a defect region. For dislocations (see below) a linear response, $\sigma(r) = \omega r$, is expected, where ω is a constant. One also might anticipate this to be a more general result, arising from the small r limit in a Taylor's expansion of an elastic response to any defect. This relationship describes a rotation with a rms angle, ω, known as the 'mosaicity'. As r increases, $\sigma(r)$ increases without bound unless the defect displace-
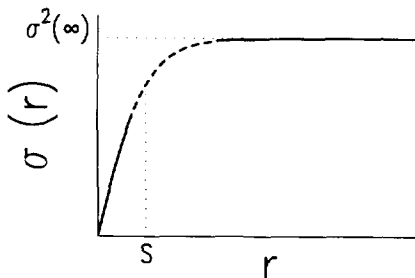
Fig. 2. Plot which schematically illustrates the expected behavior of the displacement-difference correlation function, as described in the text.

ment fields are limited by an effective spacial range or correlation length, S. For $r \gg S$, the displacements are uncorrelated and the height difference correlation function attains a constant value: $\sigma(\infty)$ reflects the rms average of all defect displacements. The intermediate length scale $r \gtrsim S$, indicated by the dashed portion of the curve in Fig. 2, is the range in which correlations *between* defects can take place. For example, if the dislocations are approximately equally spaced along the interface one would expect the dashed curve to exhibit at least one peak instead of the monotonic behavior in Fig. 2. This could lead to peaks in the diffuse scattering. The extent to which these rotational and correlation effects can be observed depend on $\sigma(\infty)$, as we now illustrate.

Limit of strong disorder: $Q_z^2 \sigma^2(\infty) \gg 1$. In this case, $e^{-Q_z^2 \sigma^2(\infty)} \ll 1$ and the only contribution to the integral in $\Gamma_{diff}(Q)$ comes from $r \ll S$ where we can use $\sigma(r) = \omega r$. Assuming azimuthal isotropy we obtain

$$\Gamma_{diff}(Q) = \frac{1}{2\pi} \int_0^\infty dr\, r J_0(q_p r) e^{-Q_z^2 \omega^2 r^2}$$

$$= \frac{1}{2\pi Q_z^2 \omega^2} \int_0^\infty dv\, v J_0(\beta v) e^{-v^2},$$

(2)

where $J_0(x)$ is the zero-order Bessel function, $\beta = q_p / Q_z \omega = \Delta\theta/\omega$ and $\Delta\theta$ is the angular tipping of the sample from the specular condition (see Fig. 1 inset). Since the integral vanishes for $\beta \gg 1$, the condition of $\beta \sim 1$ characterizes the width of the diffuse scattering and allows us to draw some general conclusions: (1) As a function of perpendicular momentum transfer, Q_z, the diffuse scattering width is constant in *angle*; (2) the angular width is equal to the mosaicity, ω; (3) the limit of strong disorder restricts the diffuse scattering to probe (see Fig. 2) only the short-range correlations related to the linear displacement field – thus, one would not expect to observe defect–defect correlation effects in this regime; (4) this model is semi-quantitative in that it can make a reasonable prediction for the diffuse line width but not for the line shape. The specific line shape obtained from the integral in Eq. (2) is a mathematical artifact of assuming in Eq. (1b) that the displacements are a Gaussian random variable. Clearly, for $r \ll S$ one expects that the displacements follow an elastic response within the defect region. However, the condition of $\beta \sim 1$ is based on scaling relationships, independent of the line shape, and one is able to predict the width of the scattering.

Limit of weak disorder: $Q_z^2 \sigma^2(\infty) \ll 1$. In this case, $e^{-Q_z^2 \sigma^2(\infty)} \approx 1$ and we can expand the exponential containing the displacements in Eq. (1a) to first order,

assuming $Q_z u \ll 1$, giving

$$\Gamma_{\text{diff}}(\mathbf{Q}) = \frac{Q_z^2 \sigma^2(\infty)}{2\pi} \int_0^\infty dr\, r J_0(q_p r)\left[1 - \frac{\sigma^2(r)}{\sigma^2(\infty)}\right] \qquad (3)$$

$$= \frac{Q_z^2 \sigma^2(\infty) S^2}{2\pi} \int_0^\infty dv\, v J_0(\beta v) C(v),$$

where $C(r/S) = [1 - [\sigma^2(r)/\sigma^2(\infty)]]$ vanishes for $r \gg S$. Here, $\beta = q_p S$ and the diffuse scattering width is again characterized by the condition that $\beta \sim 1$. We can draw some general conclusions: (1) As a function of perpendicular momentum transfer, Q_z, the diffuse scattering exhibits a constant parallel momentum transfer width, $\Delta q_p \sim 1/S$ which is characteristic of the defect correlation length; (2) Because the integral in Eq. (3) utilizes the full curve in Fig. 2, one expects that defect–defect correlations can produce structure in the diffuse scattering. The far tails of the diffuse scattering (large q_p) will reflect the intra-defect correlations whereas the region nearer to the specular scattering (small q_p) may contain information on inter-defect correlations; (3) If the displacement fields in Eq. (1a) are sufficiently small $(Q_z u \ll 1)$, then Eq. (3) follows without the assumption of Gaussian random variables and the line shape predicted by Eq. (3) is correct. Then the line shape depends on the details of $C(r/S)$.

Fig. 3 summarizes the Q_z dependence of the diffuse scattering width where the dotted lines indicate the asymptotic limits of strong and weak disorder. The two experimental results in Fig. 1 are in agreement with this picture. The 240 Å film (Fig. 1(a)) exhibits very weak
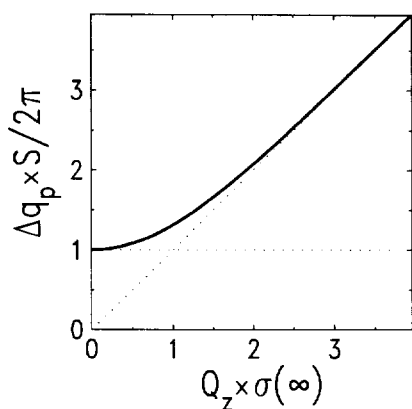
Fig. 3. The dotted curves show the asymptotic behavior of the diffuse scattering width in the limits of strong and weak disorder. The solid curve schematically shows how this might continuously evolve. All of the experimental results in Fig. 1(a) fall within the large $Q_z \sigma$ asymptotic limit whereas all the results in Fig. 1(b) fall within the small $Q_z \sigma$ limit.

specular scattering at the (0 0 2) and none at the higher order reflections, indicating that all three scans are in the strong disorder limit. Correspondingly, each of the diffuse scattering curves exhibits the same angular width. The 72 Å film (Fig. 1(b)) exhibits strong specular scattering at the (0 0 2) as well as at the (0 0 6), indicating that all data are in the weak disorder limit. In this case, the diffuse scattering width is constant in q_p, as anticipated from the model, with a correlation length of ~ 130 Å. The different behavior for the two samples is consistent with the known [9] lattice relaxation properties: the 240 Å film has a much higher dislocation density than the 72 Å film.

Recent results from X-ray studies of Nb/Al$_2$O$_3$ might also be consistent with our model. Gibaud et al. [7] found that 400 Å of Nb gave a diffuse scattering width which was constant in q_p, whereas Reimer et al. [8] studied 1500 Å of Nb and observed diffuse scattering which had a constant angular width. Given that the number of dislocations generally increases with increasing film thickness, these two results for Nb appear to follow the same trend that was observed for ErAs/GaAs and predicted by our model [14]. However, because there may be differences between samples produced in different laboratories, a systematic study of the film thickness dependence for Nb/Al$_2$O$_3$ would be useful.

It is of interest to know the physical origin of the correlation length observed in our experiments. First, we can say that it does arise from a correlation *between* dislocations. From previous X-ray studies of lattice relaxation it was found that the 72 Å film is pseudomorphic with no observable relaxation of the lattice [9]. However, the film thickness dependence of the relaxation suggests that the 72 Å film is close to showing relaxation. Using this information along with the known instrumental resolution, one can conservatively place a lower bound on the average dislocation spacing of > 1000 Å. This would give a diffuse scattering width ten times narrower than observed in Fig. 1(b). Therefore, it is likely that the diffuse scattering arises from displacements due to *isolated* dislocations and it remains to show what sets the observed length scale.

We suggest that the observed length scale, S, arises from the dislocation image field which should be significant in very thin films. One expects that the strain fields from the dislocation and its image cancel at long lateral distances so that the strain field is localized. The characteristic length scale for this cancelation is set by the film thickness so that S should be on the order of the film thickness. This is certainly consistent with the observed $S \sim 130$ Å for our 72 Å film, although, a detailed investigation of this effect has not been carried out.

We now present a specific example to illustrate the phenomena. Consider a dislocation in a semi-infinite
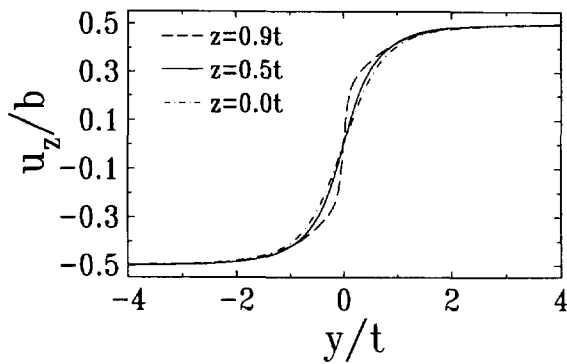
Fig. 4. Calculation of the perpendicular displacement field for a dislocation in a thin film with a free surface, as described in the text. y is the horizontal coordinate along the interface and z is the vertical coordinate perpendicular to the plane of the interface: $z = 0$ corresponds to the free surface and $z = t$ corresponds to the film/substrate interface. The condition of a stress-free surface causes the displacement field to saturate on a lateral length scale corresponding to the film thickness.

isotropic elastic medium and located a distance, t, from a stress-free surface. t can be regarded as the film thickness if we ignore the difference in elastic constants between the film and substrate (this approximation permits the discussion to focus on the effect of the stress-free surface). Fig. 4 shows the perpendicular displacement field assuming a Burgers vector, b, oriented perpendicular to the surface [15]. There are three important observations: (1) the displacement field saturates when $|y| > t$, demonstrating the scaling with film thickness; (2) the region of changing displacement field is mostly linear, suggesting a rotational-type local displacement; and (3) the displacement profile is nearly independent of z, essentially giving vertically homogeneous strain as observed experimentally. Although, this example may not correspond to the actual defects in ErAs we expect that, qualitatively, features (1) and (3) are due to the elastic response of a defect near a stress-free surface and are independent of the particular details of the defect.

In conclusion, we have identified some of the scaling relationships that determine the reflectivity in thin films containing defects. This is an important first step towards a future model that could quantitatively fit the observed shapes. For example, utilizing the limits of strong and weak disorder can greatly simplify calculations. These results also present the exciting prospect of experimentally determining dislocation strain fields at a level of detail that could not be previously achieved. Unlike large crystals, the morphology of misfit dislocations localized at the film/substrate interface can be controlled.

Acknowledgements

References

[1] W.H. Zachariasen, Theory of X-ray Diffraction in Crystals (Dover, New York, 1967); G.E. Bacon, Neutron Diffraction (Oxford University Press, Oxford, 1975).

[2] M.A. Krivoglaz, Theory of X-ray and Thermal-Neutron Scattering By Real Crystals (Plenum, New York, 1969).

[3] P.F. Miceli and C.J. Palmstrøm, Phys. Rev. B 51 (1995) 5506.

[4] P.M. Reimer, H. Zabel, C.P. Flynn and J.A. Dura, Phys. Rev. B 45 (1992) 11 426; J. Cryst. Growth 127 (1993) 643.

[5] A. Stierle, A. Abromeit, N. Metoki and H. Zabel, J. Appl. Phys. 73 (1993) 4808.

[6] A. Gibaud, R.A. Cowley, D.F. McMorrow, R.C.C. Ward and M.R. Wells, Phys. Rev. B 48 (1993) 14463.

[7] A. Gibaud, D.F. McMorrow and P.P. Swaddling, unpublished manuscript.

[8] P.M. Reimer, H. Zabel, C.P. Flynn and K. Ritley, unpublished manuscript.

[9] P.F. Miceli, C.J. Palmstrøm and K.W. Moyers, Appl. Phys. Lett. 58 (1991) 1602; P.F. Miceli, K.W. Moyers and C.J. Palmstrøm, Mat. Res. Soc. Symp. Proc. 202 (1991) 579.

[10] C.J. Palmstrøm, N. Tabatabaie and S.J. Allen, Appl. Phys. Lett. 53 (1988) 2608.

[11] P.F. Miceli, C.J. Palmstrøm and K.W. Moyers, Appl. Phys. Lett 61 (1992) 2060; P.F. Miceli, C.J. Palmstrøm and K.W. Moyers, in: Surface X-ray and Neutron Scattering, eds. H. Zabel and I.K. Robinson (Springer, Berlin, 1992) p. 203.

[12] P.F. Miceli, in: Semiconductor Interfaces Microstructures and Devices: Properties and Applications, ed. Z.C. Feng (IOP, Bristol, 1993) p. 87.

[13] S.K. Sinha, E.B. Sirota, S. Garoff and H.B. Stanley, Phys. Rev. B 38 (1988) 2297.

[14] It is to be noted that our model gives a conventional mosaic crystal in the limit of very strong disorder and such mosaic scattering is often observed in thin films. For example, see V. Hôly, J. Kubena, E. Abramof, K. Lischka, A. Pesek and E. Koppensteiner, J. Appl. Phys. 74 (1993) 1736.

[15] J.P. Hirth and J. Lothe, Theory of Dislocations (Wiley, New York, 1982).